Original Article

Inhibition of CaMKK2 Enhances Fracture Healing by Stimulating Indian Hedgehog Signaling and Accelerating Endochondral Ossification[†]

Running Title: CaMKK2 Inhibition Accelerates Bone Healing

Justin N. Williams (MS)[1], Anuradha Valiya Kambrath (MS)[1], Roshni B. Patel (BS)[1], Kyung Shin Kang (PhD)[1], Elsa Mével (PhD)[1], Yong Li (MD)[1], Ying-Hua Cheng (MD., PhD)[2], Austin J Pucylowski (BS)[1], Mariah A. Hassert (BS)[3], Michael J. Voor (PhD)[4, 5], Melissa A. Kacena (PhD)[1, 6], William R. Thompson (PhD)[7], Stuart J. Warden (PhD)[1, 7], David B. Burr (PhD)[1], Matthew R. Allen (PhD)[1,2,6], Alexander G Robling (PhD)[1] and Uma Sankar (PhD)[1,*]

[1]Department of Anatomy and Cell Biology, Indiana University School of Medicine, Indianapolis, IN
[2]Department of Medicine, Indiana University School of Medicine, Indianapolis, IN
[3]Department of Molecular Microbiology and Immunology, Saint Louis University School of Medicine, Saint Louis, Missouri
[4]Department of Orthopaedic Surgery, University of Louisville School of Medicine, Louisville, KY;
[5]Department of Bioengineering, University of Louisville Speed School of Engineering, Louisville, KY;
[6]Department of Orthopaedic Surgery, Indiana University School of Medicine, Indianapolis, IN;
[7]Department of Physical Therapy, School of Health and Rehabilitation Sciences, Indiana University, Indianapolis, IN.

[*]**To whom correspondence should be addressed**: Uma Sankar, Ph.D., Department of Anatomy and Cell Biology, Indiana University School of Medicine, 635 Barnhill Drive, MS-5055, Indianapolis, IN 46202 USA. Tel: (317) 274-7870, Fax: (317) 856-5710; Email: usankar@iupui.edu

Additional Supporting Information may be found in the online version of this article.

Initial Date Submitted September 29, 2017; Date Revision Submitted December 18, 2017; Date Final Disposition Set December 29, 2017

This is the author's manuscript of the article published in final edited form as:

Williams, J. N., Kambrath, A. V., Patel, R. B., Kang, K. S., Mével, E., Li, Y., Cheng, Y.-H., Pucylowski, A. J., Hassert, M. A., Voor, M. J., Kacena, M. A., Thompson, W. R., Warden, S. J., Burr, D. B., Allen, M. R., Robling, A. G. and Sankar, U. (2018), Inhibition of CaMKK2 Enhances Fracture Healing by Stimulating Indian Hedgehog Signaling and Accelerating Endochondral Ossification. J Bone Miner Res. Accepted Author Manuscript. http://dx.doi.org/10.1002/jbmr.3379

ABSTRACT

Approximately ten percent of all bone fractures do not heal, resulting in patient morbidity and healthcare costs. However, no pharmacological treatments are currently available to promote efficient bone healing. Inhibition of Ca^{2+}/calmodulin (CaM)-dependent protein kinase kinase 2 (CaMKK2) reverses age-associated loss of trabecular and cortical bone volume and strength in mice. In the current study, we investigated the role of CaMKK2 in bone fracture healing and show that its pharmacological inhibition using STO-609 accelerates early cellular and molecular events associated with endochondral ossification, resulting in a more rapid and efficient healing of the fracture. Within 7 days post-fracture, treatment with STO-609 resulted in enhanced Indian hedgehog signaling, *paired*-related homeobox (PRX1)-positive mesenchymal stem cell recruitment, chondrocyte differentiation and hypertrophy, along with elevated expression of osterix, vascular endothelial growth factor and type 1 collagen at the fracture callus. Early deposition of primary bone by osteoblasts resulted in STO-609 treated mice possessing significantly higher callus bone volume by 14 days following fracture. Subsequent rapid maturation of the bone matrix bestowed fractured bones in STO-609 treated animals with significantly higher torsional strength and stiffness by 28 days post-injury, indicating accelerated healing of the fracture. Previous studies indicate that fixed and closed femoral fractures in the mice take 35 days to fully heal without treatment. Therefore, our data suggest that STO-609 potentiates a 20% acceleration of the bone healing process. Moreover, inhibiting CaMKK2 also imparted higher mechanical strength and stiffness at the contralateral cortical bone within 4 weeks of treatment. Taken together, the data presented here underscore the therapeutic potential of targeting CaMKK2 to promote efficacious and rapid healing of bone fractures and as a mechanism to strengthen normal bones.

This article is protected by copyright. All rights reserved

INTRODUCTION

Fractures associated with osteoporosis and acute trauma result in significant medical costs and compromise the overall health and well-being of patients. More than 2 million osteoporotic fractures occur each year in the United States, and their numbers are expected to surpass 3 million by 2025, with a projected economic burden of over $25 billion annually in healthcare costs.[1,2] Even in healthy people, musculoskeletal injuries are associated with substantial immobility while healing, causing a loss of productivity.[3,4] For instance, a classic tibial fracture with intramedullary stabilization requires 3 to 6 months to completely heal.[5] Furthermore, 5-10% of the 8 million fractures occurring annually in the United States result in delayed or non-union, further contributing to patient suffering and medical costs.[6-8]

The process of normal fracture repair consists of four overlapping stages: 1) hematoma and initial inflammation; 2) soft callus formation; 3) hard callus formation/initial bony union, and; 4) bone remodeling/secondary bone formation.[9-12] Most fractures heal by a combination of intramembranous and endochondral ossification [10,11]. Intramembranous bone formation, where progenitors directly differentiate into matrix-secreting osteoblasts, occurs at the periosteal and endosteal surfaces, first along the proximal and distal edges of the callus and eventually covering the entire callus periphery, essentially forming a “hard callus”.[11,13] In contrast, endochondral ossification occurs at the less mechanically stable regions juxtaposed to the fracture gap, where progenitors differentiate into chondrocytes that undergo hypertrophy and produce cartilage that calcifies, forming a “soft callus”. Thereafter, osteoblast precursors are recruited into the perichondrial regions of the callus, coinciding with vascular invasion, which stimulates remodeling of the calcified matrix. Osteoprogenitors differentiate into osteoblasts and form the primary bone within the callus.[11,13-15] Recent studies suggest an alternative mechanism of cartilage to bone transition wherein hypertrophic chondrocytes at the fracture callus express pluripotency genes and transdifferentiate into osteoblasts in a process regulated by the invading vasculature.[14] Once formed, the primary bone becomes remodeled through a process where the initial bony callus is replaced with

secondary bone, which is remodeled further into a strong cortical bone that bridges the central fracture gap and becomes capable of supporting mechanical loads.[10-12]

The majority of fractures readily heal via the above processes. However, there is an ongoing need to discover pathways that influence them and develop therapeutic agents that efficiently hasten bone healing as to shorten healing time. One pathway which may influence fracture healing involves the Ca^{2+}/ CaM-dependent protein kinases (CaMKs) and, in particular, Ca^{2+}/calmodulin (CaM)-dependent protein kinase kinase 2 (CaMKK2). CaMKs are a family of multifunctional serine/threonine protein kinases that includes CaMKK1 (α), CaMKK2 (β), CaMKI, CaMKII and CaMKIV.[16-19] The CaMK signaling cascade is initiated by transient increases of intracellular Ca^{2+} and includes CaMKKs 1 and 2, as well as their downstream substrates CaMKs I and IV.[20] In addition, CaMKK2 phosphorylates and activates adenosine monophosphate activated protein kinase (AMPK) to coordinate cellular energy balance [21-24]. Consequently, inhibition or loss of CaMKK2 in mice protects from diet-induced obesity, insulin resistance, and inflammatory responses.[25-27] CaMKK2 also has roles in the anabolic and catabolic pathways in bone metabolism.[28,29] Mice lacking CaMKK2 (*Camkk2*$^{-/-}$) have more active osteoblasts, fewer osteoclasts and increased bone mass compared to wild-type (WT) mice.[28] Moreover, pharmacological inhibition of CaMKK2 using its selective cell-permeable inhibitor, STO-609, protects from ovariectomy-induced osteoporosis and stimulates a reversal of age-associated decline in trabecular and cortical bone volume and strength in 8-month old male mice. [28-32] STO-609 serves as an excellent tool to pharmacologically block CaMKK2 activity *in vitro* and *in vivo*. At lower concentrations, STO-609 is highly specific to CaMKK2 *in vivo*, does not cross the blood-brain barrier and elicits no overt toxicity.[31,33-35]

Based on previous studies indicating a potent bone anabolic activity following inhibition of CaMKK2 using STO-609, we hypothesized that targeting CaMKK2 would accelerate bone healing following injury. Our findings indicated a marked acceleration of cellular and molecular processes associated with endochondral ossification, including enhanced Indian hedgehog (IHH) signaling, PRX1-positive

mesenchymal stem cell recruitment, chondrocyte differentiation and hypertrophy, osterix (OSX), vascular endothelial growth factor (VEGF) as well as type 1 collagen (COL1) expression at the central callus, all within 7 days post-fracture. Advancement of these key early healing related processes allowed for a more rapid and robust bone formation such that the STO-609 treated calluses contained more bone with improved mechanical properties by 28 days post-fracture. Taken together, our findings indicate that the inhibition of CaMKK2 accelerates bone regeneration at the site of injury, resulting in faster and more efficient healing of the fracture.

MATERIALS AND METHODS

Mice and treatment: All animal procedures were performed with prior approval from Indiana University School of Medicine Institutional Animal Care and Use Committee (IACUC) and the Department of Defense Animal Care and Use Review Office (ACURO). All experiments were performed in compliance with NIH guidelines on the use and care of laboratory and experimental animals. Eight-week-old male C57BL6/J mice were purchased from Jackson Laboratories (Bar Harbor, ME) and housed in the Indiana University School of Medicine Laboratory Animal Resource Facility (LARC) under a 12-h light, 12-h dark cycle for 2 weeks. Food and water were provided *ad libitum*. Tri-weekly intraperitoneal (IP) injections of HBSS (Hank's Balanced Salt Solution), referred to herein as vehicle (VEH), or STO-609 (10 µmol/kg mouse body weight) were administered from the day after surgery and continued for 4 weeks post-fracture. STO-609 was purchased from TOCRIS Bioscience (Ellsville, MO, USA) and prepared as reported previously.[28]

Study Design: The current study was designed to reveal whether fracture healing is accelerated following pharmacological inhibition of CaMKK2. Fractured animals were randomly distributed into two groups: vehicle only (n=44) and STO-609 only (n=44). Sample sizes were determined based on previous fracture studies by other groups [36] and based on judgement of biological importance. Sample sizes were

determined as follows: micro-computed tomography (micro-CT) imaging, n = 10 per group on days 14 and 28; Mechanical testing, n = 10 per group on day 28; immunofluorescence and qRT-PCR, n=3/group/assay on days 3, 7 and 14. Endpoint for the study was at day 28, and was determined via micro-CT analysis of fractured and contralateral intact femurs harvested at 14 and 28 days post-fracture. Four samples per group that had displaced fractures were excluded from micro-CT analysis, resulting in a final sample size of n=6/group for this assay. Following micro-CT analysis, samples were processed for undecalcified plastic histology. Mechanical testing, micro-CT, histology and immunohistochemisty analyses were performed in a blinded manner. There were no outliers in the analyses. Statistical information is outlined in the "Statistical Analysis" section.

Fracture induction: Unilateral fractures were generated on the right femurs of 10 week old male C57BL6/J mice based on the method described by McBride-Gagyi et al.[37] Briefly, mice were anesthetized with a mixture of ketamine (100 mg/kg) and xylazine (10 mg/kg) administered via the intraperitoneal (IP) route and given a preoperative dose of buprenorphine hydrochloride analgesia (0.03 mg/kg) subcutaneously. An incision was made over the knee joint and the patella manually dislocated before inserting a 25 gauge (0.56 mm diameter) stainless steel hypodermic needle retrograde through the distal condyle of the femur. A 36 gauge (0.13 mm diameter) tungsten guidewire was then passed through the needle, the position of the needle and guidewire confirmed by radiography (piXarray 100; Micro Photonics Inc., Allentown, PA), following which the 25 gauge needle was removed. With the guidewire in place, closed femoral fractures were generated using a 3-point bending device (as described in rats by Bonnarens and Einhorn, 1986; [38]). The location of the fractures were confirmed by X-ray, following which a 24 gauge (0.51 mm) stainless steel hypodermic tubing was passed over the guide wire to internally stabilize the fractured femur. A final X-ray was performed to confirm the position of the steel tubing, the guidewire removed and the wound sutured close. Buprenorphine was administered every 12 h for 3 days, and as needed thereafter.

Micro-computed tomography (µCT) imaging: Fractured and contralateral intact femurs were excised at 14 and 28 days post-fracture and fixed in 4% paraformaldehyde (PFA; Polysciences, Warrington, PA) for 48 h at 4ºC and transferred to 70% ethanol. Micro-CT imaging was performed on both femurs at a 9 µm voxel size using Bruker 1176 µCT system (70kV, 137mA, 0.5 rotation step, 0.5 Aluminum filter). Reconstructed µCT images (NRecon software) were analyzed using CT Analyzer software (Skyscan, Kontich, Belgium). Contralateral femoral midshafts were analyzed using cross-sections approximately 3.7 mm proximal to the distal growth plate. Analysis of the fracture callus was performed with an ROI defined as a total of 4.2 mm surrounding the callus midpoint. Callus maturity was measured using differential thresholding in which immature (soft callus) bone was defined by threshold of 0.166 - 0.847 g/cm3 (842-3604 Hounsfield units) and mature (cortical) bone at a threshold greater than 0.847 g/cm3, as described previously.[39] Three-dimensional models and videos were generated using CTVox software (Skyscan, Kontich, Belgium).

Histology: Samples were embedded in poly-methyl methacrylate (plastic) for longitudinal sectioning and stained with Picrosirius Red (PSR) or Von Kossa and McNeal's (VKM). Safranin O fast green staining: cryosections were rehydrated in water, incubated in Safranin-O (0.1%), counter stained with Fast Green (0.1%) and mounted with Super Cryo Mounting Media (SCMM, Section-lab).

Immunofluorescence and Immunohistochemistry: Femurs were harvested at days 3, 7 and 14 post-fracture, fixed in 2% PFA for 48 h and transferred to 30% sucrose solution for an additional 48 h. The samples were embedded in optimal cutting temperature (OCT) compound and frozen in N-Hexane (-72°C). Using a cryomicrotome (Leica CM1950, Wetzlar, Germany), 8 µm sections were collected on a cryofilm tape (Section-lab Co. Ltd., Japan) and stored at -20°C. Sections were thawed at room temperature for 5 min, rehydrated in 1 X phosphate buffered saline (PBS) for 10 min, followed by permeabilization with 0.2% Tween20 for 5 min and incubation in Tris-Glycine mixture (0.1 M glycine (pH 7.4) in1 M Tris base) for 30 min to quench auto-fluorescence. The sections were then washed in 1 X PBS and blocked with normal donkey serum (3% BSA and 5% NDS in 1 X PBS) for 1 h. Antigen

retrieval with 1 % hyaluronidase (1: 4 dilution) for 30 min was performed for COL10 and with citrate buffer for 30 min at 50°C for IHH. Samples were incubated with appropriate dilutions of primary antibody in blocking buffer at 4^0C overnight; COL10 (234196, Millipore, St. Louis, MO, 1:200), COL1 (Millipore, AB765P, 1:50), PRX1 (TA803116, Origene, Rockville, MD, 1:50), VEGF (sc-7269, Santa Cruz Biotechnology, Dallas, TX, 1:50) Osterix (ab94744, Abcam, Cambridge, United kingdom, 1:50), and IHH (PA5-42706, Thermofisher Scientific, Hampton, NH, 1:100). Following three washes in 1 X PBS, sections were incubated the appropriate secondary antibody for 2 h in the dark; Alexa Fluor488 (1:200), Alexa Fluor594 (1:400) (both from Jackson Immunoresearch, West Grove, PA). Sections were stained with DAPI (D9542, Sigma, St. Louis, MO, 1:1000 dilution from a stock of 5mg/ml) for 10 min and mounted with Vectashield mounting medium (H-1000,Vector Laboratories, Burlingame, CA). Images were captured with Leica DMi8 fluorescent microscope and processed with Leica LAS-X software. Mean relative intensity of fluorescence in each image is quantified using ImageJ software (NIH). Fluorescence intensity (IF) values were blindly measured and averaged from 4 randomized regions of interest per callus (n=3/group).

Quantitative RT-PCR: Fractured femurs were extracted at days 3, 7 and 14 after surgery, trimmed to isolate the callus (days 3, 7 and 14). Immediately following extraction, the callus was flash frozen in liquid nitrogen and transferred to -80°C. Samples were homogenized in TRIzol (Invitrogen) using the Bullet Blender Storm (Next Advance, Averill Park, NY) with NAVY RINO homogenization tubes (Next Advance). Total RNA was isolated according to the manufacturer's protocol for TRIzol. RNA samples were treated with DNAse I (Ambion, Carlsbad, CA, USA) for 20 min at 37ºC to remove genomic DNA contamination and inactivated with DNAse I Inactivation Buffer (Ambion). RNA concentrations were determined using the BioPhotometer spectrophotometer (Eppendorf, Hauppague, NY). cDNA was synthesized from 2 µg RNA using a high capacity reverse transcriptase kit (Applied Biosystems, Waltham, MA, USA) and each sample was diluted 1:3 and prior to qPCR (final concentration of 50ng/15uL reaction). All qPCR reactions were performed using iTaq Universal SYBR Green Supermix

and the CFX Connect™ Real-Time PCR Detection System (Biorad, Hercules, CA). For a complete list of forward and reverse primers used in qPCR reactions, please refer to Table 1. Relative expression to *Gapdh* was determined via the 2^-ΔΔCt method included in the CFX Manager Software (Biorad).

Mechanical testing: Fractured and contralateral femurs were excised 28 days post-fracture, wrapped in PBS soaked gauze and frozen at -20°C. On day of testing samples were thawed at room temperature. Torsional properties of both fracture and contralateral bones were assessed on a low-force torsional testing device (ElectroForce TestBench, TA Instruments, New Castle, DE, USA). The proximal and distal ends of the femur were potted to each platen using low-melting metal (32.5% Bismuth, 51% Indium, 16.5% Tin). All the femurs were loaded in rotation at a fixed rotational rate of 0.5 degree/s until fracture at room temperature, and the rotation angle and torque were sampled at 10 Hz. Maximum torque and torsional stiffness were calculated from the torque-rotation angle curves.

Statistical Analysis: All values are represented as mean values ± standard deviation. Statistical comparisons among vehicle and STO-609 treated samples were performed using single factor ANOVA with post-hoc Tukey correction for comparisons across time points and/or a two-tailed Student's *t*-test for treatment comparison within a single time point (IBM SPSS statistics 24.0). Differences with p-value < 0.05 were deemed significant

RESULTS

CaMKK2 inhibition enhances bone maturity of the fracture callus

Radiographic imaging exhibited a similar pattern between VEH and STO-609 treated animals (Fig 1A). A reparative callus became visible by day 7, grew to its maximum size by day 14, and subsided thereafter. Whereas the healing pattern was similar between interventions, calluses from STO-609 treated mice appeared more radio-opaque than those from VEH treated controls (Fig 1A). The increased radio-opacity following STO-609 treatment was confirmed by micro-CT analysis of the callus at 14 and 28 days post-

fracture. As indicated by the representative 3D-reconstructed micro-CT images, calluses in STO-609 treated animals possessed 16% higher BV/TV than those in VEH-treated controls (Fig 1B-C). Further, the calluses from both interventions displayed a reduction in BV/TV by day 28 (Fig 1B-C), with the reduction being more pronounced in STO-609 treated animals due to their higher BV/TV at the earlier assessment time point (Fig 1C). There were no differences in the total callus volume (Supp. Fig 1).

A differential threshold method was utilized to assess the overall callus maturity at the fracture site on days 14 and 28 post-fracture (Fig 1Bii-iii and Supp. videos SV1-2). Callus maturity, defined based on tissue density, in VEH-treated mice increased 26% from day 14 to day 28 post-fracture (Fig 1D). In contrast, STO-609 treatment potentiated a 65% increase in callus maturity during the same period (Fig 1D). Thus, on day 28 post-fracture, the STO-609 treated calluses possessed 29% higher mature bone content compared to VEH-treated cohorts (Fig 1D and SV1-2). Taken together, these cumulative data indicate that CaMKK2 inhibition promotes early accumulation of endochondral bone within the reparative callus, which then accelerates to maturity by 4 weeks.

STO-609 advances chondrocyte hypertrophy at the fracture callus

Enhanced BV/TV by 14 days post-fracture in STO-609 treated calluses suggest acceleration of early cellular and molecular mechanisms associated with fracture healing. The earliest events following injury are hematoma formation and acute inflammation. Expression levels of mRNA of three inflammatory cytokines (tumor necrosis factor alpha (TNF-α), interleukin (IL)-1β and IL-6), interrogated at 3 days post-fracture, were not significantly different between the two interventions (Sup Fig 2). We also assessed the expression levels of transforming growth factor beta (TGF-β), a key mediator of fracture healing that is expressed early in the callus and observed no significant differences between the groups at day 3 (Sup Fig 2). These data suggest that CaMKK2 inhibition does not significantly alter acute inflammation, a crucial early event in fracture healing.

The inflammatory response leads to the recruitment of stem cells that differentiate into chondrocytes in the central regions of the callus. A cartilaginous callus bridging the fracture gap is typically observed on days 10-14 of normal healing in murine femoral fractures. As expected, the VEH treated calluses contained small patches of Safranin-O-positive cartilage close to the injury site on day 7 (Fig 2Ai). By day 14, a prominent area of densely stained cartilaginous tissue was visible along the central portion of the callus in VEH animals, extending from the fracture gap to the callus periphery (Fig 2Aiii). In contrast, extensive patches of cartilage were already visible adjacent to the fracture gap by day 7 in the STO-609 treated animals (Fig 2Aii), indicating early onset of endochondral ossification. By day 14, cartilaginous tissue in STO-609 treated calluses became markedly reduced and mostly confined to a small area next to the fracture gap (Fig 2Aiv). These data complement the micro-CT data indicating higher callus BV/TV at day 14 (Fig 1C), and suggest an acceleration of endochondral ossification at the fracture callus following CaMKK2 inhibition.

Stem cells at the fracture callus differentiate into chondrocytes that secrete type II collagen (COL2) and proteoglycans. The chondrocytes mature to express type 10 collagen (COL10), undergo hypertrophy and eventually apoptosis. The cartilage then undergoes mineralization, stabilizing the callus. Following our observation of early cartilage formation in fracture calluses treated with STO-609 (Fig 2A), we asked whether chondrocyte hypertrophy is enhanced as well. To this end, we evaluated the expression levels of COL10 by immunofluorescence in frozen callus sections prepared from two cohorts. At day 7 post-fracture, the VEH group expressed low levels of COL10, with an increase by 3-fold by day 14 (Fig 2Bi; 2Biii and Fig 2D). In contrast, COL10 expression was 6-fold higher in STO-609 treated calluses at day 7, compared to controls, before undergoing a marked reduction by day 14 post-fracture (Fig 2Bii; 2Biv and Fig 2D). We observed a similar pattern of expression of *Col10* mRNA (Fig 2F). Indeed, at day 7, STO-609 treated calluses possessed 30-fold higher *Col10* mRNA compared to VEH treated calluses. Compared to their respective levels at day 7 post-fracture, *Col10* mRNA decreased by 2.4-fold by day 14 in STO-609 treated cohorts, whereas it increased by 20-fold in VEH treated calluses (Fig 2F).

We then evaluated whether the levels of COL2, an early marker of proliferating chondrocytes, are also altered following CaMKK2 inhibition and found them to be temporally similar to COL10. Expression of COL2 peaked by day 7 and decreased substantially by day 14 in STO-609 treated calluses (Fig 2Cii; 2Civ). In contrast, calluses from VEH treated mice expressed 2-fold lower COL2 than STO-609 treated cohorts at 7 days post-fracture, followed by a modest increase in expression by day 14 (Fig 2Ci; 2Ciii and Fig 2E). We also noticed a striking difference in the spatial pattern of COL2 expression within the calluses of the two cohorts. In VEH treated mice, COL2 expression at day 7 post-fracture was mostly confined to a patch of cells along the periphery and a few cells inside the callus. By day 14, COL2 expression shifted to regions inside the central callus (Fig 2Ci; 2Cii). In contrast, in STO-609 treated calluses, COL2 expressing cells were predominantly localized to the central callus already by day 7 post-fracture. By day 14, COL2 expression became restricted to very few cells within the callus and along the periphery (Fig 2Ciii-Civ). *Col2* gene expression followed a similar pattern with STO-609 treated calluses possessing 11-fold higher mRNA levels than control at day 7 and then diminishing by 3-fold by day 14, whereas VEH treated calluses displayed a modest, albeit insignificant, increase in *Col2* during the same period (Fig. 2G).

The high mobility group transcription factor *Sox9*, a master regulator of chondrocyte differentiation, is a direct transcriptional activator of *Col2* gene expression in chondrocytes. Since STO-609 treatment significantly enhanced COL2 at the fracture callus by day 7, we predicted SOX9 levels to be elevated in these samples. We observed significantly higher SOX9 protein and mRNA expression on day 7 in STO-609 calluses, compared to the VEH group (Supp. Fig 3A-B). Spatially, most of the SOX9 expression was confined to the periosteal surface of the callus in VEH treated cohorts. However, intense SOX9 staining was observed all over the callus in STO-609 treated samples (Supp. Fig 3A). Taken together, these data indicate that CaMKK2 inhibition triggers an early influx of *Sox9*-positive progenitors that undergo differentiation into chondrocytes and rapidly advance to hypertrophy.

CaMKK2 inhibition promotes early expression of OSX at the callus

Chondrocyte hypertrophy and cartilage calcification stimulates the induction of angiogenesis-related genes such as vascular endothelial growth factor (VEGF), which in turn acts as a chemoattractant for the influx of mesenchymal stem cells as well as osteoprogenitors from the periosteum into the callus. We hypothesized that the presence of enhanced chondrocyte hypertrophy would stimulate early induction of VEGF within the calluses of STO-609 treated mice. Indeed, by 7 days post-fracture, the STO-609 treated calluses possessed 2.1-fold higher VEGF-positivity compared to the VEH group (Fig 3A; 3E). Moreover, VEGF-positive cells in these samples were predominantly localized along the center of the callus extending to the fracture gap (Fig 3A). In contrast, VEGF-positive cells could be observed mostly along the periphery of the callus in VEH treated mice (Fig 3A). Further, STO-609 treated calluses expressed 5-fold higher *Vegf* mRNA compared to control, on day 7 post-fracture (Fig 3F).

Next, we assessed alterations in the mRNA and protein expression of osterix (OSX), an early transcription factor required for osteoblastogenesis. As shown in Fig. 3F, *Osx* gene expression was increased by 2.7-fold in STO-609 treated calluses at day 7 post-fracture compared to the VEH group. Similarly, OSX protein levels were 2.4-fold higher in STO-609 treated calluses than controls on day 7 post-fracture (Figs 3B; 3E). We further assessed OSX levels at 14 days post-fracture, and found it to be expressed 2.6-fold higher in STO-609 treated calluses compared to VEH treated controls (Supp. Fig 4).

Furthermore, we noticed a similarity in the pattern of VEGF (red) and OSX (green) expression especially in the cells within the day 7 STO-609 treated calluses (Fig 3C). Overlay of the two signals indicated that the vast majority of VEGF-positive cells in the central callus were also OSX-positive suggesting that the bulk of the VEGF expression at the callus of the STO-609 treated mice at day 7 post-fracture came from OSX expressing osteoblast progenitors (Fig 3C). In contrast, the overlap of VEGF and OSX expression, albeit limited, was most evident at the callus periphery in VEH treated samples (Fig 3C). These data are consistent with previous reports that osteoblasts express elevated levels of *Vegf* during fracture healing.[11]

Recent studies have indicated that the osteoblasts and chondrocytes within the fracture callus originate from a common multipotent stem cell/progenitor population from the periosteum that expresses *paired*-

related homeobox gene *Prx1*.[40-44] PRX1 expression in the STO-609 treated callus was 2.5-fold higher, and its mRNA levels were 5-fold higher than those in VEH treated calluses at 7 days post-fracture (Supp. Figs 5Ai; 5Aii; 5C and 5E). By day 14, we observed a significant decrease in PRX1 protein in the central callus of STO-609 treated mice, whereas the mRNA remained elevated (p=0.06) (Supp. Figs 5Aiii; 5Aiv; 5C and 5E). We also examined the levels of Nestin, a marker of perivasculature-associated stem cells that gives rise to osteoprogenitors.[45-47] Interestingly, Nestin levels remained similar in the two cohorts at all the time points examined (Supp. Figs 5B; 5D and 5F), indicating that it is mainly the Prx1-positive stem/progenitor cells that are enhanced by CaMKK2 inhibition at the fracture callus. Thus, CaMKK2 inhibition results in an early increase of PRX1 expressing stem/progenitor cells as well as VEGF expressing, OSX-positive osteoprogenitors at the callus by the first week of bone injury.

Early upregulation of IHH signaling in CaMKK2-inhibited fracture calluses

Our data thus far beg the question of what signaling mechanism may be stimulated by CaMKK2 inhibition, early enough during the healing process, which would then orchestrate the acceleration of endochondral ossification and secondary bone formation observed in STO-609 treated calluses. One such mechanism could be the IHH signaling pathway, which is necessary for formation of the endochondral skeleton during embryonic development and bone healing.[48-53] Studies from knockout mouse models demonstrate the absolute requirement of IHH in chondrocyte maturation, osteoblast differentiation and cartilage vascularization during embryonic skeletal development.[15,50] The importance of IHH in fracture healing was recently demonstrated.[53] Therefore, we investigated whether IHH protein and mRNA levels are altered early in the reparative callus following CaMKK2 inhibition. Our results indicate that compared to controls, calluses from STO-609 treated mice possessed 2.5-fold higher levels of IHH by 7 days post-fracture, compared to VEH controls (Figs 4Ai-Aiii), and its expression was very intense in regions within the central callus closer to the fracture gap (Fig 4A). Interestingly, *Ihh* mRNA was higher by 25-fold in calluses of STO-609 treated animals by day 7 post-fracture, compared to controls (Fig 4B). To further understand if the elevation in *Ihh* following CaMKK2 inhibition occurred earlier in the healing

process, we assessed its levels at 3 days post fracture and found it to be elevated by 2-fold in STO-609 treated calluses compared to control (Fig 4B). We then evaluated the expression of IHH target genes *Patched1 (Ptch1)* and *Gli1* to understand if the IHH signaling cascade pathway is activated at the fracture callus by CaMKK2 inhibition. [50,54] Indeed, at 7 days post-fracture, *Gli1* and Ptch1 were expressed 2.5-fold and 6.5-fold higher in STO-609 treated calluses compared to controls (Figure 4C-D). At 3 days post fracture, *Ptch1* mRNA was 1.5-fold higher (p=0.06) in STO-609 treated samples, whereas *Gli1* levels were similar between the cohorts (Fig. 4C-D). Altogether, these data indicate that the inhibition of CaMKK2 stimulates an early upregulation of the IHH signaling cascade at the fracture callus, which is associated with the rapid healing.

STO-609 treatment potentiates increased matrix mineralization at the fracture callus

Initial bone healing involves endochondral ossification of the soft callus, a process executed by osteoblasts via their synthesis and mineralization of bone matrix. Mature osteoblasts secrete many matrix proteins including type 1 collagen (COL1), the major component of bone matrix. We surmised that the calluses from STO-609 treated mice would express enhanced levels of *Col1* mRNA and protein earlier in the healing process. Indeed, we observed enhances COL1 expression in calluses from STO-609 treated mice compared to VEH treated mice in both days 7 and 14 post-fracture (Figs 5A). At day 7 post-fracture, COL1 protein and *Col1* mRNA expression were significantly higher in STO-609 treated calluses than control (Figs 5B-C). COL1 levels were still higher at day 14 in STO-609 treated calluses, whereas *Col1* mRNA was not different between groups at this time point. Furthermore, we observed a difference in the spatial pattern of COL1 expression between the calluses from the two cohorts at day 14 (Fig 5A). Accordingly, COL1 expression in calluses of VEH treated animals was largely excluded from the central area juxtaposed to the fracture gap, which mostly consisted of cartilage (compare Fig 5A and 2A). In contrast, intense COL1 expression was observed in the central region of the callus in STO-609 treated samples (Fig 5A; compare low and higher magnification), similar to the pattern of OSX expression (Supp. Fig 4A). Further, examination of higher magnification images of these sections revealed the presence of

regions of intense COL1 staining, resembling mineralized tissue, along the periphery of STO-609 treated calluses (Fig 5A). These observations suggest the presence of enhanced bone matrix within the callus and mineralized bone along the callus periphery by day 14 post-fracture following treatment with STO-609.

To confirm this, we stained serial sections of day 14 calluses from both cohorts with von Kossa-McNeil (VKM) and picrosirius red (PSR) to visualize the presence of mineralized bone and lamellar structures along the callus periphery (Figs 6A-C). Compared to VEH treated controls, STO-609 treated calluses possessed a thicker strip of mineralized matrix bordering the fracture callus (Fig 6A). Higher magnification images of VKM stained calluses allow for a better, albeit qualitative, appreciation of not only the wider mineralized bone bordering the STO-609 treated callus, but also an organized osteoid surface juxtaposed to the border (Fig 6A). Moreover, histomorphometric measurements reveal the presence of 2.8-fold more osteoid along the peripheral callus surface in STO-609 treated mice (Fig 6C). Further, observation of PSR-stained sections under circular polarized light revealed the presence of dense lamellar structures along the periphery of STO-609 treated calluses compared to VEH treated cohorts (Fig 6B). These qualitative and quantitative observations, altogether, suggest that CaMKK2 inhibition results in the formation of organized, mineralized bone along the callus periphery earlier in the healing process potentially providing stability at the fracture callus.

STO-609 imparts higher torsional strength to fractured and contralateral bone

We hypothesized the acceleration of early cellular and molecular events associated with bone healing coupled with enhanced matrix deposition and maturation following CaMKK2 inhibition would impart greater strength to the healed fracture. To test this, we measured the axial torsion to failure of the reparative callus at day 28 post-fracture. STO-609 treated samples possessed an 80% greater ultimate torque (Fig 7A) and a 62% greater torsional stiffness (Fig 7B) compared to the VEH group. We then assessed whether STO-609 treatment alters geometry and strength at the contralateral femur mid-shaft. Contralateral (left) femurs from mice treated with STO-609 possessed a 28% increase in the mid-shaft polar area moment of inertia compared to control (Table 2). Further, STO-609 treated contralateral mid-

shafts possessed 44% higher ultimate torque and 40% higher torsional stiffness compared to the VEH group (Fig 7A-B). Taken together, these findings suggest treatment with STO-609 results in improved mechanical competence of healed fractures as well as improved properties of the unperturbed bone.

DISCUSSION

In this study, we show that the inhibition of CaMKK2 using its selective pharmacological inhibitor STO-609 results in a dramatic acceleration of early molecular and cellular events associated with bone fracture healing. Most interestingly, CaMKK2 inhibition results in an early upregulation of the IHH signaling cascade with higher *Ihh* mRNA observed as early as 3 days and significantly elevated *Ihh*, *Gli1* as well as *Ptch1* gene expression by 7 days post-fracture. This increased IHH signaling correlated with a rapid differentiation of SOX9-positive progenitors into the chondrocyte lineage in STO-609 treated fracture calluses. Subsequent upregulation of COL10 and chondrocyte hypertrophy, set in motion a cascade of downstream events that included an early influx into the callus of OSX-positive osteoprogenitors that expressed high levels of VEGF, which also induces neo-vascularization. Acceleration of these early molecular events associated with bone healing augmented endochondral ossification, as evidenced by enhanced COL1 expression in the callus as early as day 7 and increased primary bone deposition by day 14 post-fracture. Subsequent formation of a hard callus bridging the central fracture gap and along the callus periphery were also enhanced by CaMKK2 inhibition, contributing to increased stabilization of the fracture. Indeed, fractured femurs from STO-609 treated mice possessed significantly higher torsional strength and stiffness compared to controls by week 4 of bone healing. Altogether, our results identify CaMKK2 as an efficacious therapeutic target to hasten bone healing (Fig 8).

A closed femur fracture in the mouse, fixed with an intramedullary rod takes an average of 35 days for complete healing.[9] This is equivalent to a 3-month healing period for acute lower limb fractures in healthy humans.[55] In the mouse, the early inflammation period starts immediately after fracture and lasts

for 7 days post-injury. This is immediately followed by endochondral ossification, where chondrocyte hypertrophy and calcified cartilage formation peak during days 10-16 post-fracture. Primary and secondary bone deposition, and the subsequent coupled remodeling phase all occur during days 17-35 post-fracture.[9] Our results from this study show that following CaMKK2-inhibition using STO-609, chondrocyte differentiation and hypertrophy as well as COL2 and COL10 expression, all peak by day 7 following fracture and become downregulated thereafter. PRX1-positive MSCs, OSX-positive osteoprogenitors and VEGF expression are all significantly enhanced in the central callus by 7 days post fracture, indicating early stimulation of primary bone formation, as evidenced by the enhanced COL1 expression and higher bone callus content by day 14 in STO-609 treated calluses. This acceleration of endochondral ossification by day 7 and bony callus formation by day 14 post-fracture stimulates the advancement of the coupled remodeling phase that ultimately results in faster bridging of the fracture gap, imparting greater torsional strength to the fracture site by 28 days post-fracture. Thus, by accelerating key early molecular events, CaMKK2 inhibition potentiates a 20% acceleration of the bone healing process.

What is the mechanism for this acceleration of endochondral ossification at the fracture gap aided by CaMKK2 inhibition? Of particular interest is our observation of a dramatic increase in *Ihh* mRNA and protein very early in the healing process in STO-609-treated calluses. Compared to controls, IHH protein was increased by 2.5-fold and its mRNA levels were elevated by 2.6-fold by day 3 and an impressive 25-fold by day 7, indicating that the inhibition of CaMKK2 stimulates *Ihh* expression. IHH is a morphogen produced by pre- and early hypertrophic chondrocytes that is required for the onset of chondrocyte maturation as well as osteoblast differentiation.[48-50,52,53] During bone healing, *Ihh* mRNA is expressed at the fracture callus by pre-hypertrophic and hypertrophic chondrocytes as well as perichondrial osteoblasts, where it is proposed to advance cartilage deposition, neovascularization and osteogenesis.[49,51] The importance of IHH in fracture healing was recently demonstrated in a mouse model of diabetes mellitus, a metabolic disease characterized by impaired bone healing.[53,56,57] Delayed bone healing in these mice was associated with chronic inflammation-mediated downregulation of IHH in

skeletal stem cells and progenitors. Administration of recombinant IHH into these mice restored the osteogenic potential of skeletal stem cells and rescued bone healing.[53] The fact that STO-609 treatment also significantly elevates two downstream target genes of IHH viz., *Gli1* and *Ptch1*, by 2.5- and 6.5 fold respectively, indicates that CaMKK2 inhibition results in an early upregulation of IHH signaling at the fracture callus. We postulate this initiates the acceleration of key cellular events associated with endochondral ossification, including chondrocyte hypertrophy, influx of OSX-positive osteoblast progenitors, vascularization, and primary as well as secondary bone formation.

How might CaMKK2 regulate IHH signaling at the fracture callus? Although the exact mechanism remains to be identified, one possibility is through an indirect mechanism involving a close family member, CaMKII. Both CaMKII and CaMKK2 are activated by transient increases in intracellular Ca^{2+} downstream of phospholipase C (PLC) signaling, which in turn is activated by the heterotrimeric G protein Gq/11.[58,59] However, CaMKII is not part of the CaMK signaling cascade that has CaMKK2 at its apex.[60] Ectopic activation of CaMKII in developing chick wings is associated with enhanced *Ihh* and *Col10* mRNA as well as chondrocyte hypertrophy, driven in part by increased RUNX2, with *Ihh* mRNA being its direct transcriptional target.[61,62] Whereas the exact role of CaMKII in chondrocytes remains elusive, parathyroid hormone-related peptide (Pthrp) and Wnt5a/Frizzled 7 signaling both downregulate CaMKII through dephosphorylation during chondrocyte proliferation.[61,63] Of note, we previously reported that CaMKII and CaMKIV, a direct downstream target of CaMKK2, play mutually antagonistic roles in myeloid leukemia cells.[64] When taken together, these studies provide credence to the possibility of an inhibitory crosstalk between CaMKK2 and CaMKII as one of the mechanisms driving enhanced IHH signaling and endochondral ossification at the fracture callus following CaMKK2 inhibition.

While the endochondral ossification-mediated repair process occurs at the central fracture callus, mineralized bone matrix, or a hard callus, is formed along the callus periphery by intramembranous ossification to provide structural stability to the reparative callus.[9,11,13] STO-609 treated fracture calluses displayed intense COL1 expression along the callus periphery by 7 days post-injury, and its levels further

increased and encompassed most of the callus by day 14. Furthermore, these calluses possessed enhanced mineralized bone along the callus periphery by day 14 post-fracture, which when coupled with increased content of mature bone in the callus by day 28, imparted superior strength to the repaired bone. Of note, we observed increased expression of the periosteal stem cell marker PRX1along the callus periphery as early as 7 days post-fracture. These data suggest that in addition to its role in accelerating endochondral ossification, CaMKK2 inhibition may also stimulate the differentiation and/or activity of OSX/COL1-expressing osteoblasts at the callus periphery.

Additionally, the fact that contralateral mid-shafts displayed significantly higher polar moment of inertia, torsional stiffness and strength following four-weeks of STO-609 treatment is of particular interest and it indicates stimulation of anabolic activity by osteoblasts along the cortical bone following CaMKK2 inhibition. We previously reported that treating 32-week old mice with a 6-week course of STO-609 stimulated new bone formation and significantly increased both trabecular and cortical bone mass and strength, indicating a substantial anabolic effect.[29] Thus, CaMKK2 inhibition could help strengthen bone as a strategy of fracture prevention in the elderly as well as in military personnel and athletes.

Age-associated complications, life-style choices such as smoking and underlying metabolic or endocrine abnormalities deleteriously influence bone healing, often resulting in delayed or nonunion of fracture, imposing a tremendous burden on the healthcare system and patients, economically and in terms of quality of life.[6,9] Delayed union and non-union fractures are often associated with a persistent cartilage callus that is either delayed or impaired in its conversion to bone.[65] Whereas therapies that heal recalcitrant fractures are crucial, strategies that strengthen the bone and/or hasten the healing time in healthy individuals are also of tremendous importance. For example, in the military, acute musculoskeletal injuries during active combat significantly delay the return of soldiers to active duty and stress fractures incurred during training are among the leading causes of attrition of personnel, especially women, early in their career.[3,4] Moreover, in older individuals with osteoporosis, it is well-documented that a prior fracture doubles the risk of subsequent fractures.[66] Unfortunately, there are no

pharmacological agents currently approved for the acceleration of fracture healing, treatment of delayed union or non-union, or for strengthening the bone altogether as a prevention strategy. Through the early upregulation of IHH, CaMKK2 inhibition accelerates endochondral ossification in the central callus, by advancing chondrocyte hypertrophy, osteoprogenitor influx as well as primary and secondary bone deposition. By simultaneously stimulating COL1-expressing mature osteoblasts to actively secrete bone matrix that matures into a hard callus that imparts high torsional strength and stiffness to the fractured bone, CaMKK2 inhibition orchestrates a rapid and efficient healing of bone fractures. Additionally, the anabolic activity associated with inhibiting CaMKK2 stimulates gaining of strength at the contralateral cortical bone, potentially preventing future fragility fractures. Altogether, the data presented here identify CaMKK2 as an attractive therapeutic target for accelerating fracture healing, promoting fracture gap union and strengthening the intact bone as a prevention strategy.

ACKNOWLEDGEMENTS

The authors thank Dr. Keith W. Condon for help with histology and guidance on immunohistochemistry, Drs. Ushashi Dadwal and Mavis Irwin for technical assistance. **Funding**: This work was supported by grants from the Department of Defense (DoD) US Army Medical Research and Materiel Command (USAMRMC) Congressionally Directed Medical Research Programs (CDMRP) (PR121604) to US as well as National Institutes of Arthritis and Musculoskeletal and Skin Diseases (NIAMS), NIH R01 AR068332 to US and AR053237 to AGR. JNW is supported through a Comprehensive Musculoskeletal T32 Training Program from NIAMS/NIH (AR065971 to DBB). The 1176 µCT system was supported by an S10 grant (NIH - OD016208 to MRA). **Author contributions**: US conceived and supervised the study, designed the experiments, analyzed data and wrote the manuscript; JNW assisted in the design and performed experiments, analyzed data, made figures and wrote the manuscript; ANV performed immunohistochemistry, analyzed data, wrote manuscript, RBP performed qRT-PCR, analyzed data and made figures; EM performed qRTPCR and data analysis; KSK performed the biomechanical testing; AJP

analyzed X-ray and micro-CT images; YL and Y-HC performed surgeries and assisted with data analysis; MAH performed experiments and analyzed images; MJV assisted with study design and edited the manuscript, MJV, MAK, WRT, SJW, DBB, MRA assisted in data analysis, provided critical input on data interpretations and edited the manuscript; MRA also assisted with micro-CT analyses, generated supplementary videos from micro-CT data; AGR supervised and performed the torsional strength testing, data analysis; helped edit the manuscript.

Grant Support: This work was supported by grants from the Department of Defense (DoD) US Army Medical Research and Materiel Command (USAMRMC) Congressionally Directed Medical Research Programs (CDMRP) (PR121604) to US as well as National Institutes of Arthritis and Musculoskeletal and Skin Diseases (NIAMS) R01 AR068332 to US and AR053237 to AGR. JNW is supported through a Comprehensive Musculoskeletal T32 Training Program from NIAMS/NIH (AR065971 to DBB). The 1176 µCT system was supported by an S10 grant (NIH - OD016208 to MRA).

Disclosures

All authors of this manuscript state that they have no conflict of interest. The authors further state that there are no restrictions on full access for all authors to all raw data, statistical analyses and material used in the study reported in this manuscript.

REFERENCES

1. Schnell S, Friedman SM, Mendelson DA, Bingham KW, Kates SL. The 1-Year Mortality of Patients Treated in a Hip Fracture Program for Elders. Geriatric Orthopaedic Surgery & Rehabilitation. 2010;1(1):6-14.
2. Burge R, Dawson-Hughes B, Solomon DH, Wong JB, King A, Tosteson A. Incidence and economic burden of osteoporosis-related fractures in the United States, 2005-2025. J Bone Miner Res. Mar 2007;22(3):465-75.
3. Covey DC, Aaron RK, Born CT, Calhoun JH, Einhorn TA, Hayda RA, et al. Orthopaedic war injuries: from combat casualty care to definitive treatment: a current review of clinical advances, basic science, and research opportunities. Instr Course Lect. 2008;57:65-86. Epub 2008/04/11.
4. Kahanov L, Eberman LE, Games KE, Wasik M. Diagnosis, treatment, and rehabilitation of stress fractures in the lower extremity in runners. Open Access Journal of Sports Medicine. 03/27 2015;6:87-95.
5. Busse JW, Bhandari M, Einhorn TA, Schemitsch E, Heckman JD, Tornetta P, et al. Re-evaluation of low intensity pulsed ultrasound in treatment of tibial fractures (TRUST): randomized clinical trial. BMJ. 2016;355.
6. Cunningham BP, Brazina S, Morshed S, Miclau T, III. Fracture healing: A review of clinical, imaging and laboratory diagnostic options. Injury.48:S69-S75.
7. Einhorn TA. Can an anti-fracture agent heal fractures? Clin Cases Miner Bone Metab. Jan 2010;7(1):11-4. Epub 2010/01/01.
8. Hak DJ, Fitzpatrick D, Bishop JA, Marsh JL, Tilp S, Schnettler R, et al. Delayed union and nonunions: epidemiology, clinical issues, and financial aspects. Injury. Jun 2014;45 Suppl 2:S3-7.
9. Einhorn TA, Gerstenfeld LC. Fracture healing: mechanisms and interventions. Nat Rev Rheumatol. Review 01//print 2015;11(1):45-54.
10. Schindeler A, McDonald MM, Bokko P, Little DG. Bone remodeling during fracture repair: The cellular picture. Semin Cell Dev Biol. Oct 2008;19(5):459-66.
11. Ai-Aql ZS, Alagl AS, Graves DT, Gerstenfeld LC, Einhorn TA. Molecular mechanisms controlling bone formation during fracture healing and distraction osteogenesis. Journal of dental research. Feb 2008;87(2):107-18. Epub 2008/01/26.
12. Gerstenfeld LC, Alkhiary YM, Krall EA, Nicholls FH, Stapleton SN, Fitch JL, et al. Three-dimensional Reconstruction of Fracture Callus Morphogenesis. Journal of Histochemistry & Cytochemistry. November 1, 2006 2006;54(11):1215-28.
13. Dimitriou R, Tsiridis E, Giannoudis PV. Current concepts of molecular aspects of bone healing. Injury. Dec 2005;36(12):1392-404.
14. Hu DP, Ferro F, Yang F, Taylor AJ, Chang W, Miclau T, et al. Cartilage to bone transformation during fracture healing is coordinated by the invading vasculature and induction of the core pluripotency genes. Development. Jan 15 2017;144(2):221-34.
15. Maes C, Kobayashi T, Selig MK, Torrekens S, Roth SI, Mackem S, et al. Osteoblast precursors, but not mature osteoblasts, move into developing and fractured bones along with invading blood vessels. Dev Cell. Aug 17 2010;19(2):329-44.
16. Colomer J, Means AR. Physiological roles of the Ca2+/CaM-dependent protein kinase cascade in health and disease. Sub-cellular biochemistry. 2007;45:169-214.
17. Kitsos CM, Sankar U, Illario M, Colomer-Font JM, Duncan AW, Ribar TJ, et al. Calmodulin-dependent protein kinase IV regulates hematopoietic stem cell maintenance. The Journal of biological chemistry.Sep 30 2005;280(39):33101-8. Epub 2005/07/16.

18. Kokubo M, Nishio M, Ribar TJ, Anderson KA, West AE, Means AR. BDNF-mediated cerebellar granule cell development is impaired in mice null for CaMKK2 or CaMKIV. J Neurosci. Jul 15 2009;29(28):8901-13. Epub 2009/07/17.

19. Means AR. The Year in Basic Science: calmodulin kinase cascades. Molecular endocrinology.Dec 2008;22(12):2759-65. Epub 2008/10/11.

20. Anderson KA, Means RL, Huang QH, Kemp BE, Goldstein EG, Selbert MA, et al. Components of a calmodulin-dependent protein kinase cascade. Molecular cloning, functional characterization and cellular localization of Ca2+/calmodulin-dependent protein kinase kinase beta. J Biol Chem. Nov 27 1998;273(48):31880-9.

21. Anderson KA, Means AR. Central control of feeding. F1000 Biol Rep. 2009;1:10. Epub 2009/01/01.

22. Green MF, Anderson KA, Means AR. Characterization of the CaMKKbeta-AMPK signaling complex. Cell Signal. Dec 2011;23(12):2005-12.

23. Hurley RL, Anderson KA, Franzone JM, Kemp BE, Means AR, Witters LA. The Ca2+/calmodulin-dependent protein kinase kinases are AMP-activated protein kinase kinases. J Biol Chem. Aug 12 2005;280(32):29060-6. Epub 2005/06/28.

24. Hawley SA, Pan DA, Mustard KJ, Ross L, Bain J, Edelman AM, et al. Calmodulin-dependent protein kinase kinase-beta is an alternative upstream kinase for AMP-activated protein kinase. Cell Metabolism. In Vitro Jul 2005;2(1):9-19. Epub 2005/08/02.

25. Racioppi L, Noeldner PK, Lin F, Arvai S, Means AR. Calcium/calmodulin-dependent protein kinase kinase 2 regulates macrophage-mediated inflammatory responses. J Biol Chem. Mar 30 2012;287(14):11579-91.

26. Anderson KA, Lin F, Ribar TJ, Stevens RD, Muehlbauer MJ, Newgard CB, et al. Deletion of CaMKK2 from the liver lowers blood glucose and improves whole-body glucose tolerance in the mouse. Mol Endocrinol. Research Support, N.I.H., Extramural Feb 2012;26(2):281-91. Epub 2012/01/14.

27. Anderson KA, Ribar TJ, Lin F, Noeldner PK, Green MF, Muehlbauer MJ, et al. Hypothalamic CaMKK2 Contributes to the Regulation of Energy Balance. Cell Metabolism. 2008;7(5):377-88.

28. Cary RL, Waddell S, Racioppi L, Long F, Novack DV, Voor MJ, et al. Inhibition of Ca(2)(+)/calmodulin-dependent protein kinase kinase 2 stimulates osteoblast formation and inhibits osteoclast differentiation. J Bone Miner Res. Jul 2013;28(7):1599-610.

29. Pritchard ZJ, Cary RL, Yang C, Novack DV, Voor MJ, Sankar U. Inhibition of CaMKK2 reverses age-associated decline in bone mass. Bone. Jun 2015;75:120-7.

30. Sankar U, Pritchard ZJ, Voor MJ. Micro-computed tomography assisted distal femur metaphyseal blunt punch compression for determining trabecular bone strength in mice. J Biomech. May 03 2016;49(7):1233-7.

31. Tokumitsu H, Inuzuka H, Ishikawa Y, Ikeda M, Saji I, Kobayashi R. STO-609, a specific inhibitor of the Ca(2+)/calmodulin-dependent protein kinase kinase. J Biol Chem. May 3 2002;277(18):15813-8. Epub 2002/02/28.

32. Tokumitsu H, Inuzuka H, Ishikawa Y, Kobayashi R. A single amino acid difference between alpha and beta Ca2+/calmodulin-dependent protein kinase kinase dictates sensitivity to the specific inhibitor, STO-609. J Biol Chem. Mar 28 2003;278(13):10908-13.

33. Kukimoto-Niino M, Yoshikawa S, Takagi T, Ohsawa N, Tomabechi Y, Terada T, et al. Crystal Structure of the Ca2+/Calmodulin-dependent Protein Kinase Kinase in Complex with the Inhibitor STO-609. Journal of Biological Chemistry. June 24, 2011 2011;286(25):22570-9.

34. Marcelo KL, Ribar T, Means CR, Tsimelzon A, Stevens RD, Ilkayeva O, et al. Research Resource: Roles for Calcium/Calmodulin-Dependent Protein Kinase Kinase 2 (CaMKK2) in Systems Metabolism. Mol Endocrinol. May 2016;30(5):557-72.

35. York B, Li F, Lin F, Marcelo KL, Mao J, Dean A, et al. Pharmacological inhibition of CaMKK2 with the selective antagonist STO-609 regresses NAFLD. Scientific reports. Sep 18 2017;7(1):11793.

36. Liu X, McKenzie JA, Maschhoff CW, Gardner MJ, Silva MJ. Exogenous hedgehog antagonist delays but does not prevent fracture healing in young mice. Bone. 2017/10/01/ 2017;103(Supplement C):241-51.

37. McBride-Gagyi SH, McKenzie JA, Buettmann EG, Gardner MJ, Silva MJ. Bmp2 conditional knockout in osteoblasts and endothelial cells does not impair bone formation after injury or mechanical loading in adult mice. Bone. Dec 2015;81:533-43.

38. Bonnarens F, Einhorn TA. Production of a standard closed fracture in laboratory animal bone. J Orthop Res. 1984;2(1):97-101.

39. Warden SJ, Komatsu DE, Rydberg J, Bond JL, Hassett SM. Recombinant human parathyroid hormone (PTH 1-34) and low-intensity pulsed ultrasound have contrasting additive effects during fracture healing. Bone. Mar 2009;44(3):485-94.

40. Kawanami A, Matsushita T, Chan YY, Murakami S. Mice expressing GFP and CreER in osteochondro progenitor cells in the periosteum. Biochemical and biophysical research communications. Aug 28 2009;386(3):477-82. Epub 2009/06/23.

41. Martin JF, Olson EN. Identification of a prx1 limb enhancer. Genesis (New York, NY : 2000). Apr 2000;26(4):225-9. Epub 2000/04/05.

42. Murao H, Yamamoto K, Matsuda S, Akiyama H. Periosteal cells are a major source of soft callus in bone fracture. Journal of bone and mineral metabolism. Jul 2013;31(4):390-8. Epub 2013/03/12.

43. Wang T, Zhang X, Bikle DD. Osteogenic Differentiation of Periosteal Cells During Fracture Healing. Journal of Cellular Physiology. 2017;232(5):913-21.

44. Chesterman ES, Kern MJ. Comparative analysis of Prx1 and Prx2 expression in mice provides evidence for incomplete compensation. The Anatomical Record. 2002;266(1):1-4.

45. Ono N, Ono W, Mizoguchi T, Nagasawa T, Frenette Paul S, Kronenberg Henry M. Vasculature-Associated Cells Expressing Nestin in Developing Bones Encompass Early Cells in the Osteoblast and Endothelial Lineage. Developmental Cell. 2014/05/12/ 2014;29(3):330-9.

46. Rostovskaya M, Anastassiadis K. Differential Expression of Surface Markers in Mouse Bone Marrow Mesenchymal Stromal Cell Subpopulations with Distinct Lineage Commitment. PLOS ONE. 2012;7(12):e51221.

47. Méndez-Ferrer S, Michurina TV, Ferraro F, Mazloom AR, MacArthur BD, Lira SA, et al. Mesenchymal and haematopoietic stem cells form a unique bone marrow niche. Nature. Article 08/12/online 2010;466:829.

48. Hilton MJ, Tu X, Cook J, Hu H, Long F. Ihh controls cartilage development by antagonizing Gli3, but requires additional effectors to regulate osteoblast and vascular development. Development. 2005;132(19):4339-51.

49. Le AX, Miclau T, Hu D, Helms JA. Molecular aspects of healing in stabilized and non-stabilized fractures. J Orthop Res. Jan 2001;19(1):78-84. Epub 2001/05/03.

50. Long F, Chung U-i, Ohba S, McMahon J, Kronenberg HM, McMahon AP. Ihh signaling is directly required for the osteoblast lineage in the endochondral skeleton. Development. 2004;131(6):1309-18.

51. Murakami S, Noda M. Expression of Indian hedgehog during fracture healing in adult rat femora. Calcified tissue international. Apr 2000;66(4):272-6. Epub 2000/04/01.

52. St-Jacques B, Hammerschmidt M, McMahon AP. Indian hedgehog signaling regulates proliferation and differentiation of chondrocytes and is essential for bone formation. Genes & Development. August 15, 1999 1999;13(16):2072-86.

53. Tevlin R, Seo EY, Marecic O, McArdle A, Tong X, Zimdahl B, et al. Pharmacological rescue of diabetic skeletal stem cell niches. Science Translational Medicine. 2017;9(372).

54. Yang J, Andre P, Ye L, Yang Y-Z. The Hedgehog signalling pathway in bone formation. International Journal of Oral Science. 05/29 04/16/accepted 2015;7(2):73-9.

55. Marsell R, Einhorn TA. Emerging bone healing therapies. Journal of orthopaedic trauma. Mar 2010;24 Suppl 1:S4-8. Epub 2010/03/10.

56. Macey LR, Kana SM, Jingushi S, Terek RM, Borretos J, Bolander ME. Defects of early fracture-healing in experimental diabetes. JBJS. 1989;71(5):722-33.

57. Moseley KF. Type 2 diabetes and bone fractures. Current opinion in endocrinology, diabetes, and obesity. Apr 2012;19(2):128-35. Epub 2012/01/21.

58. Guo J, Chung U-I, Kondo H, Bringhurst FR, Kronenberg HM. The PTH/PTHrP Receptor Can Delay Chondrocyte Hypertrophy In Vivo without Activating Phospholipase C. Developmental Cell. 2002/08/01/ 2002;3(2):183-94.

59. Hook SS, Means AR. Ca2+/CaM-Dependent Kinases: From Activation to Function. Annual Review of Pharmacology and Toxicology. 2001/04/01 2001;41(1):471-505.

60. Racioppi L, Means AR. Calcium/calmodulin-dependent protein kinase kinase 2: roles in signaling and pathophysiology. J Biol Chem. Sep 14 2012;287(38):31658-65.

61. Li Y, Ahrens MJ, Wu A, Liu J, Dudley AT. Calcium/calmodulin-dependent protein kinase II activity regulates the proliferative potential of growth plate chondrocytes. Development (Cambridge, England). 11/15/accepted 2011;138(2):359-70.

62. Pratap J, Wixted JJ, Gaur T, Zaidi SK, Dobson J, Veeraraj KD, et al. Runx2 Transcriptional Activation of Indian Hedgehog and a Downstream Bone Metastatic Pathway in Breast Cancer Cells. Cancer research. 2008;68(19):7795-802.

63. Taschner MJ, Rafigh M, Lampert F, Schnaiter S, Hartmann C. Ca2+/Calmodulin-dependent kinase II signaling causes skeletal overgrowth and premature chondrocyte maturation. Developmental biology. May 01 2008;317(1):132-46. Epub 2008/03/18.

64. Monaco S, Rusciano MR, Maione AS, Soprano M, Gomathinayagam R, Todd LR, et al. A novel crosstalk between calcium/calmodulin kinases II and IV regulates cell proliferation in myeloid leukemia cells. Cell Signal. Feb 2015;27(2):204-14.

65. Kostenuik P, Mirza FM. Fracture healing physiology and the quest for therapies for delayed healing and nonunion. J Orthop Res. Feb 2017;35(2):213-23.

66. van Geel TACM, Huntjens KMB, van den Bergh JPW, Dinant G-J, Geusens PP. Timing of Subsequent Fractures after an Initial Fracture. Current Osteoporosis Reports. 06/18 2010;8(3):118-22.

FIGURE LEGENDS

Figure 1. CaMKK2 inhibition enhances bone volume and mature bone content of the fracture callus.

(A) Representative weekly radiographic images of mice treated with vehicle (VEH) or STO-609 (n=40/group) taken to monitor the progression of fracture healing. White arrows indicate the initial site of fracture. **(Bi)** Representative longitudinal micro-CT images of the fracture callus at 14 and 28 days post-fracture (n=6/group). **(Bii)** Three-dimensional models of the callus derived from micro-CT scans demonstrate the differential thresholding of immature (new callus) bone in gray and mature (fully mineralized) bone in red. **(Biii)** Cross sections of the previously mentioned 3D models. **(C)** Mean percent bone volume (BV/TV) of the fracture callus at 14 and 28 days post-fracture, excluding the original cortical bone and marrow cavity. **(D)** Mean callus maturity calculated as a proportion of immature and mature bone present in the healing fracture callus at 14 and 28 days post-fracture. Error bars represent standard deviation; *p*-values: * $p < 0.05$, **** $p < 0.0001$.

Figure 2. Treatment with STO-609 accelerates chondrocyte hypertrophy in the fracture callus.

(A-C) Representative images calluses treated with VEH (i, iii; n=3/group) or STO-609 (ii, iv; n=3/group) at days 7 and 14 post-fracture; stained as follows: **(A)** Cartilage was stained histochemically with safranin O fast green (SOFG; 40X magnification); cartilage - orange; other tissue including bone - green. (**B-C)** Immunofluorescence (IF) staining (100X magnification) for expression of COL10 **(B)** and COL2 **(C)**, both in green. Sections were counterstained with DAPI to visualize nuclei as blue. **(D-E)** Quantitation of mean IF intensity for COL10 **(D)** and COL2 **(E)** expression, measured using ImageJ analysis (n=3/group). **(F-G)** Normalized levels of mRNA for *Col10* **(F)** and *Col2a1* **(G)** relative to *Gapdh* (n=3/group). Error bars represent standard deviation; *p*-value: * $p < 0.05$.

Figure 3. Early upregulation of OSX and VEGF in the callus following CaMKK2 inhibition.

(A-D) Representative images (200X magnification) of 7-day old calluses treated with VEH (i; n=3) or STO-609 (ii; n=3); stained as follows: **(A)** VEGF (red): **(B)** OSX (green) and **(C)** overlay of VEGF and OSX positive cells (yellow). Sections were counterstained with DAPI to visualize nuclei as blue. **(E)** Quantitation of mean IF intensity for VEGF and OSX measured using ImageJ analysis (n=3/group). **(F)** Normalized levels of *Osx* and *Vegf* mRNA relative to *Gapdh* (n=3/group). Error bars represent standard deviation; *p*-value: * $p < 0.05$.

Figure 4. Inhibition of CaMKK2 leads to increased Indian hedgehog signaling.

(A) Representative images (100X magnification) of calluses treated with VEH (i; n=3) or STO-609 (ii; n=3) at day 7 post-fracture; stained for IHH expression in green. Sections were counterstained with DAPI to visualize nuclei as blue. **(Aiii)** Quantitation of mean IF intensity for IHH measured using ImageJ analysis (n=3/group). **(B-D)** Normalized levels of *Ihh* **(B),** *Gli1* **(C)** and *Ptch1* **(D)** mRNA relative to *Gapdh* (n=3/group) on days 3 and 7 post-fracture. Error bars represent standard deviation; *p*-value: ** $p < 0.01$, **** $p < 0.0001$.

Figure 5. STO-609 treatment enhances bone matrix formation at the fracture callus.

(A) Representative images of 7 and 14 day old calluses treated with VEH or STO-609 (n=3/group); stained for expression of COL1A1 (40X and 100X magnification; green). Sections were counterstained with DAPI to visualize nuclei as blue. **(B)** Quantitation of mean IF intensity for COL1A1 measured using ImageJ analysis (n=3/group). **(C)** Normalized levels of *Col1a1* mRNA relative to *Gapdh* (n=3/group). Error bars represent standard deviation; *p*-value: * $p < 0.05$.

Figure 5. STO-609 increases bone mineralization at the callus periphery.

(A-B) Representative images of 14 day old calluses stained with Von Kossa and McNeil's tetrachrome (**A**; VKM; 50X, 100X, 200X magnification) and picrosirius red (**B**; PSR; 400X); mineralized bone, black; osteoid, light blue; organization of collagen fibers, red. (n=6/group). **(C)** Percentage of the peripheral

callus bone surface covered with osteoid as measured using histomorphometry (n=6/group). Error bars represent standard deviation; *p*-value: * $p < 0.05$.

Figure 7. CaMKK2 inhibition imparts greater torsional strength on the fracture callus and contralateral mid-shaft.

Torsional strength of fractured and contralateral femurs treated with either VEH or STO-609 (n=10/group) 28 days after fracture was measured as follows: (A) maximum torque to failure in newton-meters of the fracture callus or contralateral mid-shaft; (B) torsional stiffness calculated from the torque-rotation angle curves. Error bars represent standard deviation; *p*-value: * $p < 0.05$, ** $p < 0.01$.

Figure 8. A model for accelerated bone fracture healing following CaMKK2 inhibition.

This diagram summarizes the events of fracture healing observed in mice treated with vehicle (left) or STO-609 (right). Pharmacological inhibition of CaMKK2 with STO-609 was associated with increased numbers of proliferating (Col2) chondrocytes by day 7 post-fracture. Concurrent expression of high levels of IHH in these calluses correlated with the presence of increased numbers of hypertrophic (Col10) chondrocytes, MSCs (Prx1) and Osx-positive osteoprogenitors along with increased VEGF expression in the central callus. Subsequently, CaMKK2-inhibited animals possessed increased levels of COL1 expression, more organized bone matrix within the callus as well as a greater proportion of mineralized bone along the callus periphery by day 14 post-fracture. By day 28, treatment with STO-609 resulted in enhanced callus maturity and strength compared to control mice, indicating rapid and efficient healing of the bone fracture following CaMKK2 inhibition.

TABLES

Table 1. List of qRT-PCR primers used in this study

Target	Forward primer: 5'-3'	Reverse primer: 5'-3'	AT
Gapdh	CCTGGAGAAACCTGCCAAGTATG	AGAGTGGGAGTTGCTGTTGAAGTC	60ºC
Ihh	TGACAGAGATGGCCAGTGAG	AGAGCTCACCCCCAACTACA	60ºC
Vegf	TGGTGACATGGTTAATCGGT	AGAAAGACAGAACAAAGCCAGA	60ºC
Prx1b	CATCGTACCTCGTCCTGCTC	GCCCCTCGTGTAAACAACAT	60ºC
Col10a1	ATGCCTTGTTCTCCTCTTACTG	TGCTGAACGGTACCAAACG	60ºC
Col2a1	TTAGAGCCATCTTTGCCAGAG	CGAGGTTTCACTGGACTGC	60ºC
Sox9	AGGTTTCAGATGCAGTGAGGAGCA	ACATACAGTCCAGGCAGACCCAAA	60ºC
Osterix	CTCCTGCAGGCAGTCCTC	GGGAAGGGTGGGTAGTCATT	60.8ºC
Col1a1	AACCTGGTGCGAAAGGTGAA	AGGAGCACCAACGTTACCAA	60ºC

AT – Annealing Temperature

Table 2. Contralateral femur mid-shaft geometry

	Femur mid-diaphysis	
	Saline	STO-609
Mediolateral inner diameter (mm)	1.37 ± 0.09	1.70 ± 0.03
Mediolateral outer diameter (mm)	1.74 ± 0.10	2.10 ± 0.03
Dorsoventral inner diameter (mm)	0.80 ± 0.03	0.88 ± 0.01
Dorsoventral outer diameter (mm)	1.13 ± 0.02	1.23 ± 0.01
Cortical bone thickness (mm)	0.35 ± 0.03	0.37 ± 0.01
Cross sectional moment of inertia (mm^4)	0.20 ± 0.04	0.34 ± 0.02*
Polar moment of inertia (mm^4)	0.36 ± 0.12	0.46 ± 0.09*

* *p*-value < 0.05; n=10/group

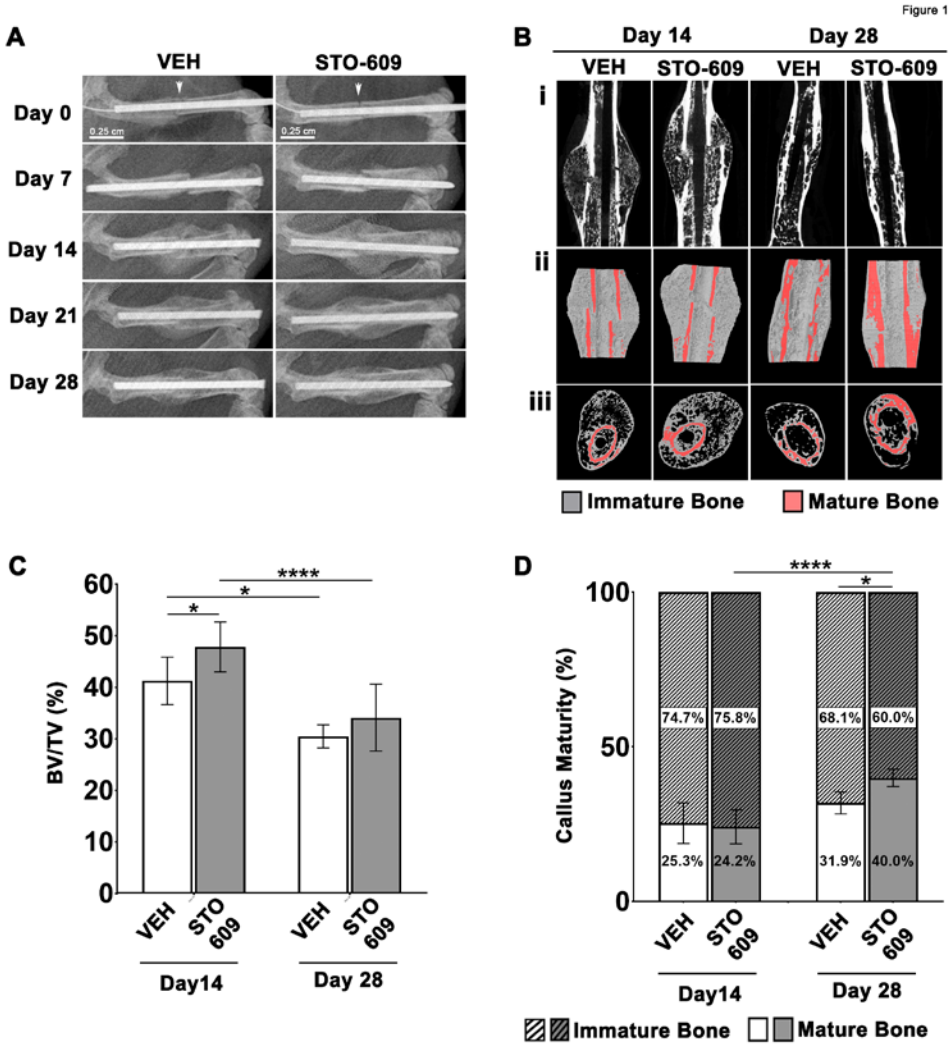

Figure 1

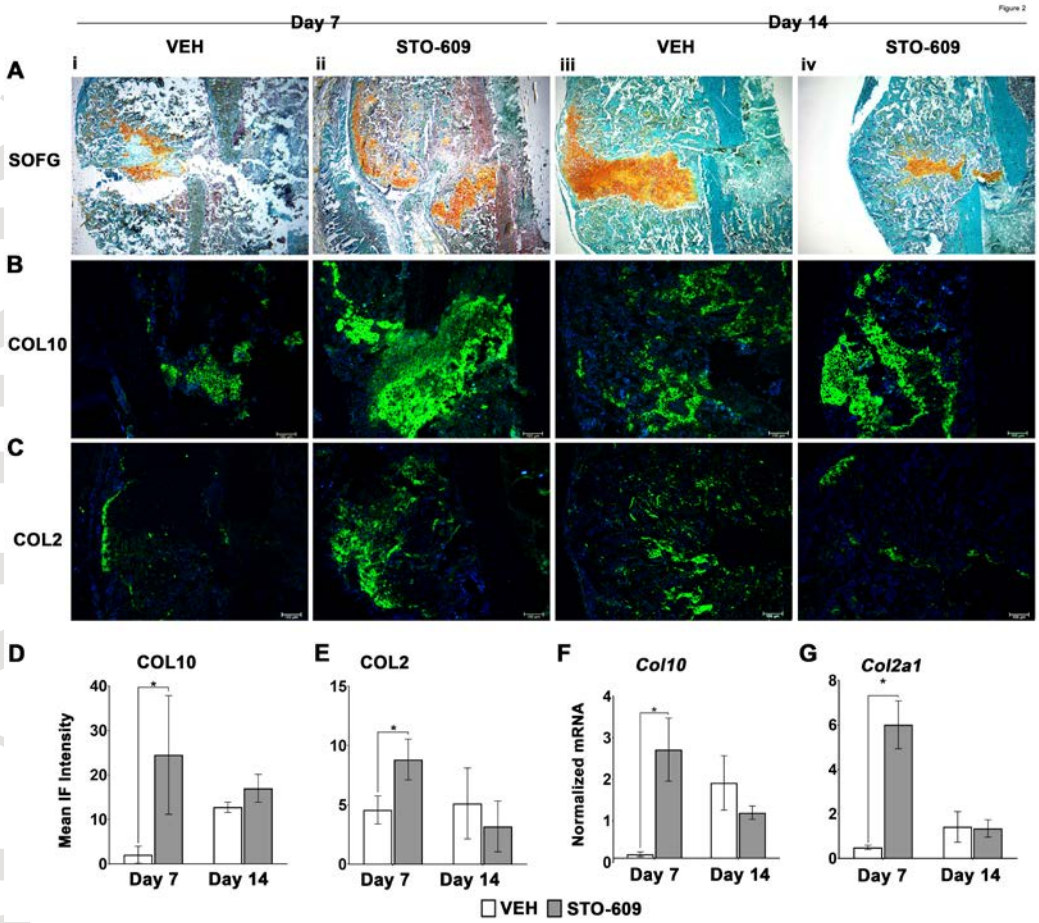

Figure 2

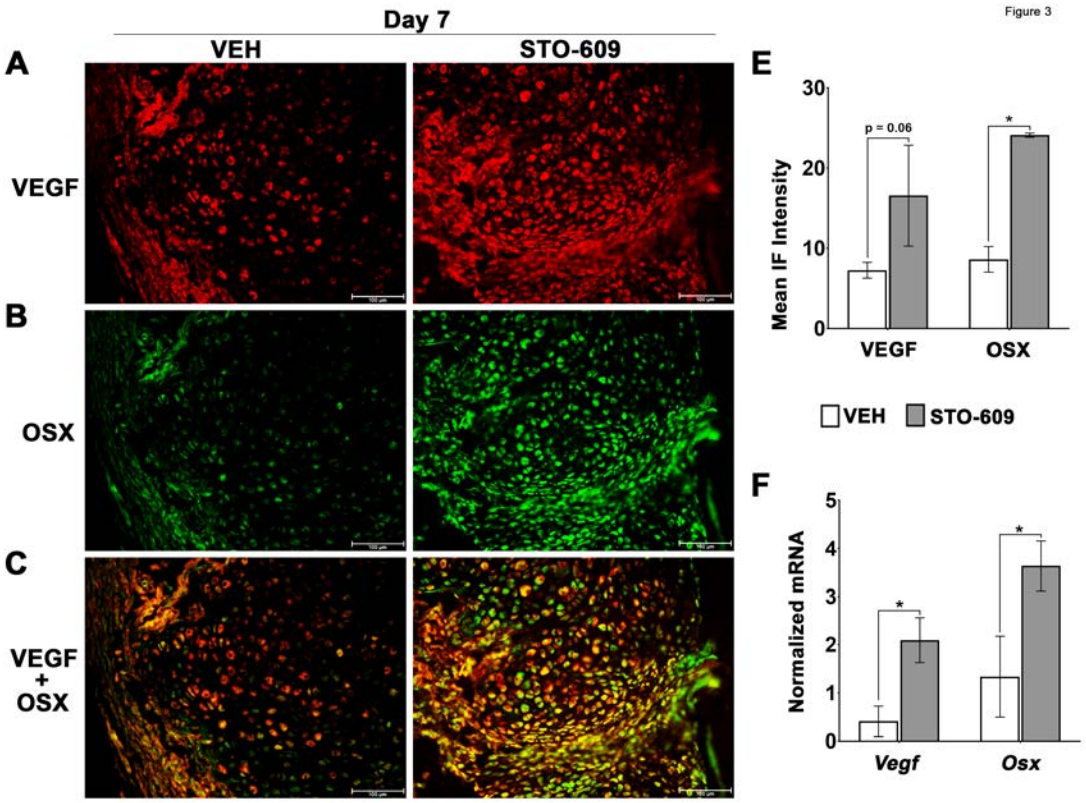

Figure 3

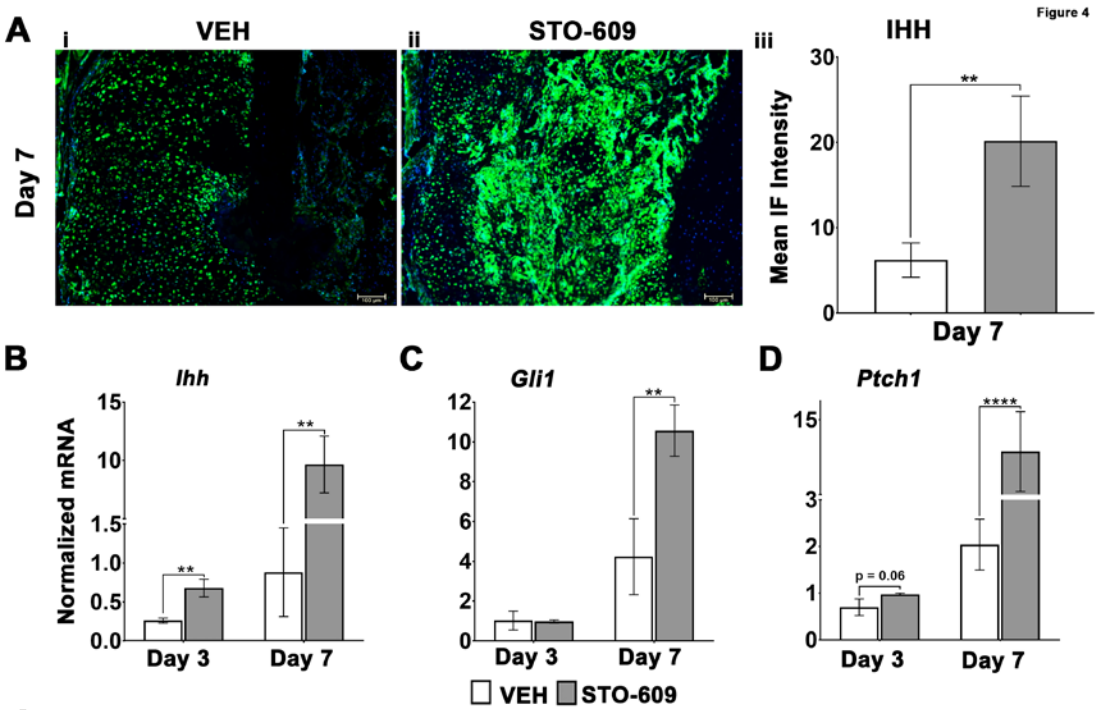

Figure 4

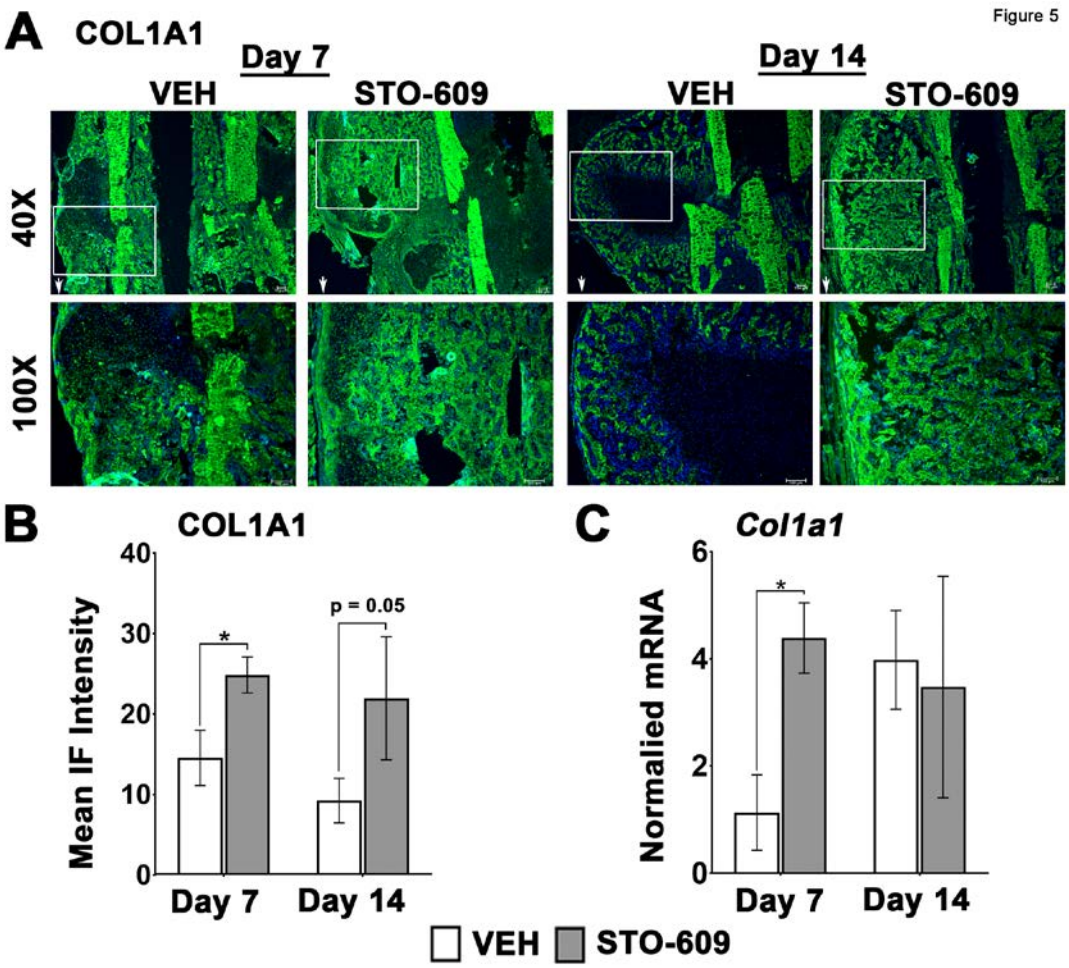

Figure 5

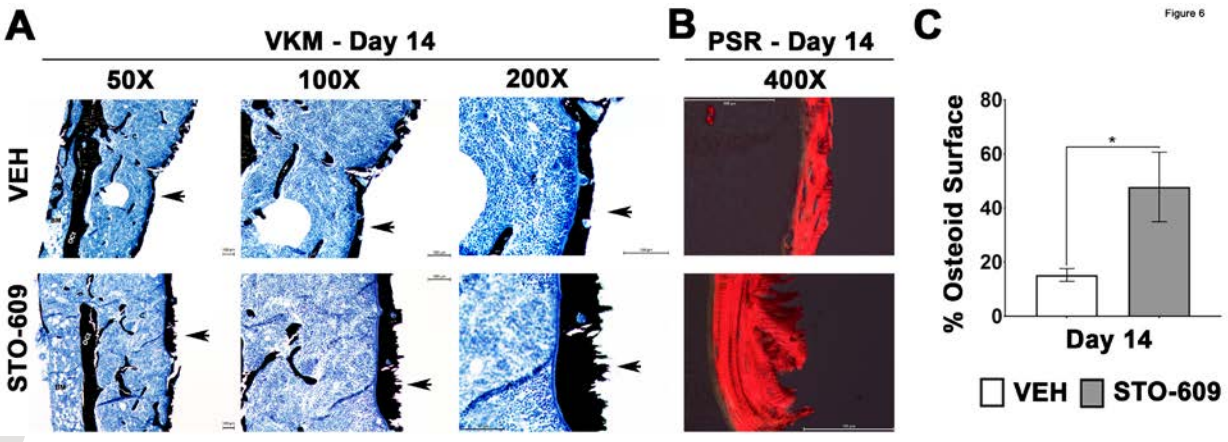

Figure 6

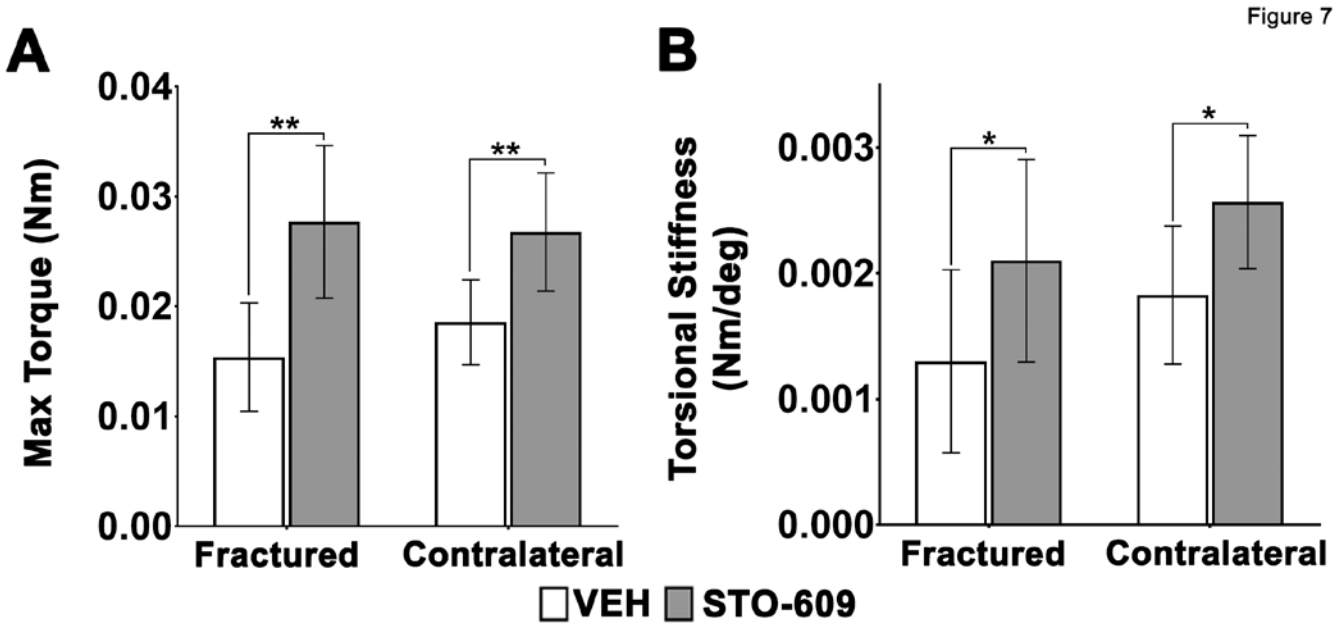

Figure 7

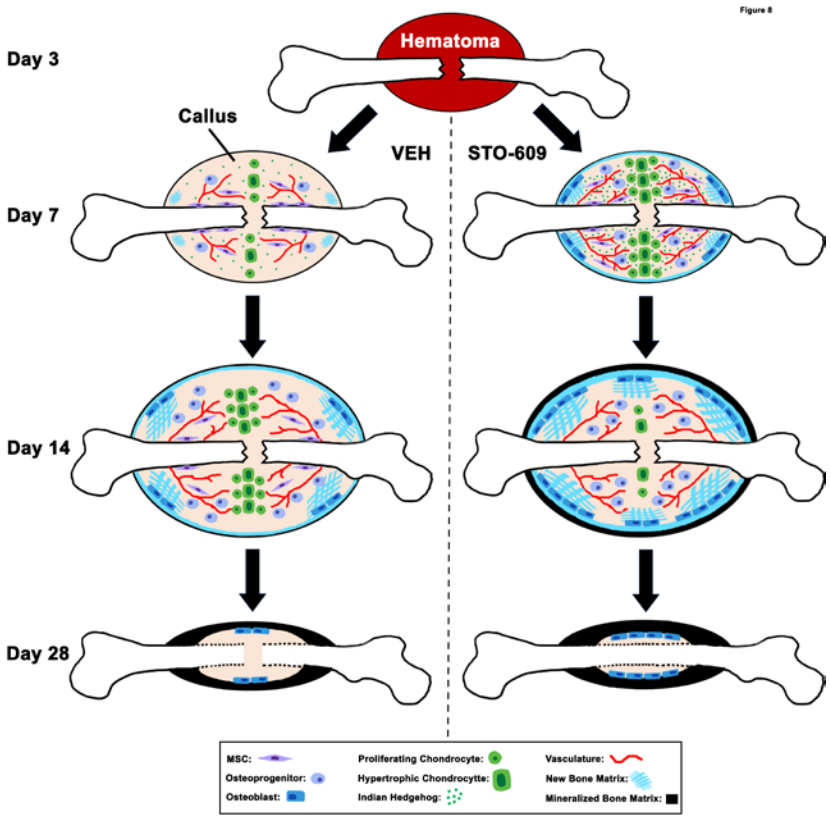

Figure 8